

# Kernel-based Greedy Approximation of Parametric Elliptic Boundary Value Problems

Bernard Haasdonk <sup>\*1</sup>, Tizian Wenzel <sup>†2</sup>, and Gabriele Santin <sup>‡3</sup>

<sup>1</sup>Institute of Applied Analysis and Numerical Simulation,  
University of Stuttgart, Germany

<sup>2</sup>Department of Mathematics, LMU Munich, Germany

<sup>3</sup>Department of Environmental Sciences, Informatics and  
Statistics, Ca' Foscari University of Venice, Italy

July 10, 2025

## Abstract

We recently introduced a scale of kernel-based greedy schemes for approximating the solutions of elliptic boundary value problems. The procedure is based on a generalized interpolation framework in reproducing kernel Hilbert spaces and was coined PDE- $\beta$ -greedy procedure, where the parameter  $\beta \geq 0$  is used in a greedy selection criterion and steers the degree of function adaptivity. Algebraic convergence rates have been obtained for Sobolev-space kernels and solutions of finite smoothness. We now report a result of exponential convergence rates for the case of infinitely smooth kernels and solutions. We furthermore extend the approximation scheme to the case of parametric PDEs by the use of state-parameter product kernels. In the surrogate modelling context, the resulting approach can be interpreted as an *a priori* model reduction approach, as no solution snapshots need to be precomputed. Numerical results show the efficiency of the approximation procedure for problems which occur as challenges for other parametric MOR procedures: non-affine geometry parametrizations, moving sources or high-dimensional domains.

**Mathematics Subject Classification (2020):** 46E22, 65D15, 65N35

## 1 Introduction

We consider general linear partial differential equation (PDE) boundary value problems (BVPs) in the strong form on arbitrary bounded Lipschitz domains. Apart from classical grid-based discretization techniques, collocation approaches have frequently been discussed in the literature. In kernel-based approximation

---

<sup>\*</sup>haasdonk@mathematik.uni-stuttgart.de

<sup>†</sup>wenzel@math.lmu.de

<sup>‡</sup>gabriele.santin@unive.it

of PDEs, a well known approach is Kansa’s method [19, 35], which results in a non-symmetric system matrix. In contrast, changing the ansatz-space for the approximants leads to symmetric collocation procedures [12] which have computational and analytical advantages. Especially these symmetric approaches can be cast in the setting of generalized interpolation [42, Chap. 16], which is an elegant and powerful framework covering many optimal recovery problems. In the context of approximating BVPs by collocation, the problem of positioning the collocation points is a central aspect determining the quality of the approximation. We refer to the PDE- $P$ -greedy procedure [36], which provides a data-independent recipe for placing the points. As a generalization, we recently presented a scale of meshless greedy kernel-based collocation techniques [48] denoted as PDE- $\beta$ -greedy procedures. The approximation spaces are incrementally constructed by carefully collecting Riesz-representers of (derivative operator) point-evaluation functionals. The scale of methods is parametrized by a parameter  $\beta \in [0, \infty]$  and naturally generalizes existing approaches of PDE approximation such as the PDE- $P$ -greedy as well as function approximation techniques such as the  $P$ -greedy [10],  $f$ -greedy [27, 37],  $f/P$ -greedy [27, 49],  $f \cdot P$  (also denoted power scaled residual (psr) method) [11], or the scale of  $\beta$ -greedy approaches [47]. We remark that point-selection methods are widely studied for the Kansa collocation method, see [23, 22, 24, 25, 20]. Moreover, another popular technique for the approximation of PDE solutions by kernels is the RBF-FD method, which is based on local differentiation stencils similarly to classical finite difference schemes. For this algorithm, the selection of interpolation and collocation points is of central importance, and several techniques have been introduced [40, 9, 39, 30, 21, 38].

General convergence statements for greedy generalized interpolation methods have been derived [2]. In contrast to those non-quantitative statements, assuming well-posedness and a stability estimate of the given BVP, we can rigorously prove convergence rates of the resulting approximation schemes [48]. Interestingly, those rates show that it is possible to break the curse of dimensionality and potentially reach high input dimensions. In the (non-PDE) function approximation context, it could be shown that those rates (for the  $f$ -greedy procedure) are optimal for certain kernels and target functions [34]. For domains in small input space dimensions the schemes can be experimentally compared with, e.g., standard finite element methods (FEM). The strength of the procedure, however, is the ease of treating high-dimensional input space dimensions due to the mesh-independence and the omission of spatial integrals. In the current article, we report a result of exponential convergence rates for the procedure in the case of smooth solutions and infinitely smooth kernels. We then extend the scheme in order to approximate parametric BVPs. The essential point here is the use of combined parameter-state kernel functions. Approximation of parametric problems is the central task in parametric model order reduction (MOR) [5] and reduced basis (RB) methods [16, 18]. The latter especially represent so called *a posteriori* MOR procedures, that make use of an offline-online decomposition, where in the offline-phase snapshots of solutions are computed in order to construct a parametric surrogate, that can be efficiently queried in an online-phase. For the case of collocation discretizations we want to mention the Reduced Collocation approaches [6] and emphasize that the online-phase for such models is non-trivial, as it requires reduced system assembly (possibly involving additional interpolation steps), and solving of corresponding (least-

squares) systems. In contrast, *a priori* MOR approaches aim at providing a global parametric surrogate as a function, that can be trivially sampled. This eliminates the classical offline-online separation, as the online-phase is essentially trivialized, and the full model computation is done in the offline phase. In this sense our overall procedure can be interpreted as an *a priori* surrogate modelling approach. Approaches such as Proper Generalized Decomposition (PGD) [29] or Physics Informed Neural Networks (PINNs) [32] are alternative methods that can provide global surrogates for parametric problems. For fixed (non-greedy) collocation point sets, recently a constrained minimum norm approximation strategy using Gaussian Processes (GPs) has been suggested and analyzed for nonlinear PDEs [7, 4]. For linear PDEs the underlying algebraic linear equation system structure is identical to ours. In this viewpoint, our method can be interpreted as a way of providing problem-adapted collocation point sets for the GP-approach. With our approach, we can especially address nontrivial parametric geometries even allowing topology changes, non-separable parameter dependencies such as moving sources, or high-dimensional domains which are inaccessible for standard grid-based methods such as FEM. These problem types pose challenges or obstacles for standard linear-subspace model reduction techniques such as RB methods.

The structure of the article is as follows. We start with recalling the kernel-based (non-parametric) PDE-greedy schemes in Sec. 2. We review existing algebraic convergence statements and present an exponential convergence result in Sec. 2.5. In Sec. 3 we extend the scheme in order to approximate parametric PDEs. Numerical results in Sec. 4 show the benefits and limitations of the approach. We conclude with some opportunities for future work in Sec. 5. An appendix contains the proof details in order to keep the main text concise.

## 2 PDE-Greedy Kernel Methods

### 2.1 PDEs

We consider BVPs for linear elliptic second order differential equations in the strong form: For a given bounded (open) domain  $\Omega \subset \mathbb{R}^d$  with boundary  $\partial\Omega$ , right-hand side (RHS) source function  $f \in C^0(\Omega) \cap L^\infty(\Omega)$  and boundary value function  $g \in C^0(\partial\Omega)$ , we want to find a solution  $u \in C^2(\Omega) \cap C^0(\bar{\Omega})$  s.t.

$$Lu(x) = f(x), \quad x \in \Omega, \quad Bu(x) = g(x), \quad x \in \partial\Omega.$$

Here  $L : C^2(\Omega) \rightarrow C^0(\Omega)$  is assumed to be a differential operator with coefficients in  $C^\infty(\Omega) \cap L^\infty(\Omega)$  and  $B : C^1(\Omega) \rightarrow C^0(\partial\Omega)$  is a suitable boundary value operator, e.g. extracting Dirichlet, Neumann or Robin boundary values, possibly with different conditions on different parts of the boundary. We assume the BVP to be well-posed, i.e. for any suitably regular  $f$  and  $g$  there exists a unique classical solution  $u$ , which depends continuously on the data via

$$\|u\|_{L^\infty(\bar{\Omega})} \leq C_L \|f\|_{L^\infty(\Omega)} + C_B \|g\|_{L^\infty(\partial\Omega)}, \quad (1)$$

with  $C_L, C_B$  independent of  $u$ . For uniformly elliptic problems this is typically guaranteed by a suitable maximum principle [33, 48].

## 2.2 Kernels and RKHSs

The approximation framework is formulated in reproducing kernel Hilbert spaces (RKHSs). For this we consider a kernel, i.e. a symmetric function  $k : \bar{\Omega} \times \bar{\Omega} \rightarrow \mathbb{R}$ , which is assumed to be strictly positive definite meaning that all kernel matrices for pairwise distinct point sets are assumed to be positive definite. Such a kernel induces an RKHS denoted  $\mathcal{H}_k(\bar{\Omega}) \subset \{h \mid h : \bar{\Omega} \rightarrow \mathbb{R}\}$  with the property that  $k(x, \cdot) \in \mathcal{H}_k(\bar{\Omega})$  and  $\langle h, k(x, \cdot) \rangle_{\mathcal{H}_k(\bar{\Omega})} = h(x)$  for all  $x \in \bar{\Omega}$  and  $h \in \mathcal{H}_k(\bar{\Omega})$  (reproducing property). For any continuous linear functional  $\lambda \in \mathcal{H}_k(\bar{\Omega})'$  we denote  $v_\lambda \in \mathcal{H}_k(\bar{\Omega})$  as its Riesz-representer. Let  $\delta_x$  denote the point evaluation functional in  $x \in \bar{\Omega}$ , i.e.  $\delta_x(h) = h(x)$  for all  $h \in \mathcal{H}_k(\bar{\Omega})$ . The definition of an RKHS implies that the point evaluation functionals are continuous and  $v_{\delta_x} = k(x, \cdot)$  is the corresponding Riesz-representer. If  $k$  is chosen as a Matérn or Wendland kernel, the corresponding RKHS is norm-equivalent to a certain Sobolev space [42]. Especially, we will apply the quadratic Matérn kernel in the experiments, i.e.

$$k_\varepsilon^M(x, x') := (3 + 3\varepsilon \|x - x'\| + \varepsilon^2 \|x - x'\|^2) \exp(-\varepsilon \|x - x'\|), \quad x, x' \in \bar{\Omega}, \quad (2)$$

with shape parameter  $\varepsilon \in \mathbb{R}_{>0}$ , which has  $C^4(\bar{\Omega} \times \bar{\Omega})$  classical regularity, its RKHS is a subset of  $C^2(\bar{\Omega})$  and is norm-equivalent to the Sobolev space  $H^{(d+5)/2}(\bar{\Omega})$ . However, in the following we will mostly focus on the infinitely smooth case, especially use the Gaussian kernel with an isotropic Euclidean distance  $k_\varepsilon^G(x, x') := \exp(-\varepsilon^2 \|x - x'\|^2)$ , or involving an anisotropic Mahalanobis distance

$$k_B^G(x, x') := \exp(-(x - x')^T B (x - x')) \quad (3)$$

for a symmetric positive definite matrix  $B \in \mathbb{R}^{d \times d}$ .

## 2.3 Generalized Interpolation

We assume that we have chosen a kernel  $k$  that matches the regularity of the solution, i.e.  $u \in \mathcal{H}_k(\bar{\Omega})$ . Then, we interpret the BVP as a collection of functional conditions: We define sets of functionals via

$$\Lambda_L := \{\delta_x \circ L \mid x \in \Omega\}, \quad \Lambda_B := \{\delta_x \circ B \mid x \in \partial\Omega\}, \quad \Lambda := \Lambda_L \cup \Lambda_B,$$

and corresponding target values  $y_\lambda := \lambda(u) \in \mathbb{R}$  for  $\lambda \in \Lambda$ . This means  $y_\lambda = f(x)$  for  $\lambda = \delta_x \circ L \in \Lambda_L$  and  $y_\lambda = g(x)$  if  $\lambda = \delta_x \circ B \in \Lambda_B$ . Then the BVP can equivalently and compactly be expressed as finding  $u \in \mathcal{H}_k(\bar{\Omega})$  such that

$$\lambda(u) = y_\lambda, \quad \lambda \in \Lambda.$$

The set  $\Lambda$  is linearly independent under the uniform ellipticity condition.

The approximation now is obtained in the setting of generalized interpolation [42, Chap. 16]. For this we assume to have chosen a set of functionals  $\Lambda_n := \{\lambda_1, \dots, \lambda_n\} \subset \Lambda$ . The corresponding trial space is set as

$$V_n := \text{span}\{v_{\lambda_1}, \dots, v_{\lambda_n}\} \subset \mathcal{H}_k(\bar{\Omega}),$$

and the approximant  $s_n \in V_n$  is obtained by requiring

$$\lambda_i(s_n) = y_{\lambda_i}, \quad i = 1, \dots, n.$$

Computationally, this corresponds to solving the following linear equation system for  $\alpha = (\alpha_i)_{i=1}^n \in \mathbb{R}^n$ :

$$K\alpha = y, \text{ with } K = \left( \langle v_{\lambda_i}, v_{\lambda_j} \rangle_{\mathcal{H}_k(\bar{\Omega})} \right)_{i,j=1}^n \in \mathbb{R}^{n \times n} \text{ and } y = (y_{\lambda_1}, \dots, y_{\lambda_n})^T \in \mathbb{R}^n,$$

and then setting  $s_n = \sum_{i=1}^n \alpha_i v_{\lambda_i} \in \mathcal{H}_k(\bar{\Omega})$ . Since the set  $\Lambda_n \subset \Lambda$  is linearly independent, this matrix  $K$  is positive definite thanks to the strict positive definiteness of the kernel. Thus a unique solution exists. Moreover this approximant  $s_n$  can be shown to be the solution of the constrained norm-minimization problem

$$\min_{s \in \mathcal{H}_k(\bar{\Omega})} \|s\|_{\mathcal{H}_k(\bar{\Omega})}^2 \quad \text{s.t.} \quad \lambda_i(s) = y_{\lambda_i}, \quad i = 1, \dots, n.$$

Finally, the approximant  $s_n$  can equivalently be characterized by an orthogonal projection, i.e.  $s_n = \Pi_{V_n}(u)$ , where  $\Pi_{V_n} : \mathcal{H}_k(\bar{\Omega}) \rightarrow V_n$  indicates the orthogonal projection operator onto  $V_n$ .

For continuous linear functionals  $\lambda \in \mathcal{H}_k(\bar{\Omega})'$  one can show that the Riesz representer is given as the functional applied to one argument of the kernel, i.e.  $v_\lambda = \lambda^{[1]}k(\cdot, \cdot)$ , where the superscript indicates application to the first argument such that the resulting object is a function only of the second argument. For the functionals of the BVP this results in  $v_\lambda = L^{[1]}k(x, \cdot)$  if  $\lambda = \delta_x \circ L \in \Lambda_L$ , and similarly for  $B$ .

Assuming w.l.o.g. that the functionals in  $\Lambda_n$  are sorted into  $n_L$  functionals from  $\Lambda_L$  and  $n_B$  from  $\Lambda_B$  and the evaluation points are denoted as  $x_{L,i}, i = 1, \dots, n_L$  and  $x_{B,i}, i = 1, \dots, n_B$ , the kernel matrix can explicitly be written in block-matrix form as

$$K = \left( \begin{array}{c|c} (L^{[1]}L^{[2]}k(x_{L,i}, x_{L,j}))_{i,j=1}^{n_L} & (L^{[1]}B^{[2]}k(x_{L,i}, x_{B,j}))_{i,j=1}^{n_L, n_B} \\ \hline (*)^T & (B^{[1]}B^{[2]}k(x_{B,i}, x_{B,j}))_{i,j=1}^{n_B} \end{array} \right),$$

where the  $(*)^T$  indicates the corresponding transpose of the right upper block. Due to the inherent symmetry of the system matrix, this PDE approximation procedure is referred to as symmetric collocation.

Moreover, the procedure recovers the standard kernel interpolation procedure for function approximation in the case of assuming  $L = \text{Id}$ ,  $B = \text{Id}$ , and hence  $\lambda_i = \delta_{x_i}$  for suitable centers  $x_i \in \bar{\Omega}$ .

An important ingredient for the subsequent scheme is the generalized power function  $P_{\Lambda_n} : \mathcal{H}_k(\bar{\Omega})' \rightarrow \mathbb{R}$  defined as

$$P_{\Lambda_n}(\lambda) := \sup_{0 \neq u \in \mathcal{H}_k(\bar{\Omega})} \frac{|\lambda(u - \Pi_{V_n}(u))|}{\|u\|_{\mathcal{H}_k(\bar{\Omega})}}, \quad \lambda \in \mathcal{H}_k(\bar{\Omega})'.$$

Observe that  $P_{\Lambda_n}(\lambda) \leq \|\lambda\|_{\mathcal{H}_k(\bar{\Omega})'}$ , since  $\Pi_{V_n}$  is an orthogonal projection, thus  $P_{\Lambda_n}$  is uniformly bounded over  $\Lambda$  if  $\Lambda$  itself is bounded in  $\mathcal{H}_k(\bar{\Omega})'$ .

The relevance of this quantity is twofold. First, introducing  $e_n := u - s_n = u - \Pi_{V_n}(u)$  as the approximation error of the collocation scheme, the definition of the power function trivially yields an error bound for functional evaluations

$$|\lambda(e_n)| = |\lambda(u - \Pi_{V_n}(u))| \leq P_{\Lambda_n}(\lambda) \|u\|_{\mathcal{H}_k(\bar{\Omega})}, \quad \lambda \in \Lambda.$$

Assuming boundedness of  $\Lambda$ , the well-posedness estimate (1) directly results in an  $L^\infty$ -error bound

$$\begin{aligned} \|u - s_n\|_{L^\infty(\bar{\Omega})} &\leq C_L \sup_{\lambda \in \Lambda_L} |\lambda(u - s_n)| + C_B \sup_{\lambda \in \Lambda_B} |\lambda(u - s_n)| \quad (4) \\ &\leq C'' \sup_{\lambda \in \Lambda} P_{\Lambda_n}(\lambda) \|u\|_{\mathcal{H}_k(\bar{\Omega})}, \end{aligned}$$

with  $C'' := \max(C_L, C_B)$ . Second, the power function is a measure of stability of the (generalized) interpolation procedure, as will be explained in the next subsection.

## 2.4 Greedy Generalized Kernel Interpolation

The number  $n$  that can practically be considered in the full collocation approach of the previous section is limited to at most a few thousand, due to several reasons. From standard kernel interpolation it is well known that the kernel matrix is in general dense, posing limitations due to quadratic memory scaling and cubic complexity for the linear system solve. Furthermore the matrix typically is ill-conditioned, which is getting more severe with increasing  $n$ . The same problems occur here, as the system matrix is obtained by evaluations of derivatives of the initial kernel, as exemplified in the previous section. Although reducing the smoothness of the kernel generally improves the conditioning of its kernel matrix, the kernel derivatives result in the scale parameters, e.g.  $\varepsilon$ , occurring as factors, which may additionally lead to worse conditioning.

A method for counteracting these problems is to turn to greedy procedures for selecting a subset of functionals. For this we assume to have a large set  $\Lambda_N \subset \Lambda$  with  $N \in \mathbb{N}$ , for which we cannot or do not want to set up the full collocation matrix, hence we rather consider this to be a set of candidate collocation functionals. We aim to incrementally select functionals  $\lambda_i \in \Lambda_N$  for  $i = 1, \dots, n$ , with  $n \ll N$ , that provide good overall approximation by collocation on a corresponding small set  $\Lambda_n \subset \Lambda_N$ .

The abstract algorithm is given in Alg. 1, which requires a kernel  $k$ , the set of functionals  $\Lambda_N$ , the vector of target values  $y_N := \Lambda_N(u) \in \mathbb{R}^N$  which means the right-hand side (RHS) functions  $f$  and  $g$  evaluated in the corresponding collocation points, as stopping criteria a maximum expansion size  $n_{max}$ , an accuracy tolerance  $\varepsilon_{acc}$  and a stability tolerance  $\varepsilon_{stab}$ . The algorithm requires a general selection criterion at iteration  $i$

$$\eta_i : \Lambda_N \rightarrow \mathbb{R}_{\geq 0},$$

which should indicate which functional is to be chosen next. The criterion can make use of the current approximation space  $V_{i-1}$  and approximant  $s_{i-1}$ . The specific choice of this selection criterion will be given later. The procedure then incrementally selects the functional that maximizes the current selection indicator. The corresponding Riesz-representer is computed, orthonormalized with respect to the current space such that the next orthonormal basis vector is obtained. The functional set and trial space are correspondingly extended and the next solution approximation computed by solving a (full) generalized kernel interpolation problem `GeneralizedKernelInterpol` on the current subset  $\Lambda_i$  as described in the previous subsection. The notation  $y_N(\Lambda_i)$  in this step is

---

**Algorithm 1** GreedyGeneralizedKernelInterpol

---

**Require:** Kernel function  $k$ , set of functionals  $\Lambda_N$ , target values  $y_N = \Lambda_N(u)$ , maximum iterations  $n_{max}$ , accuracy tolerance  $\varepsilon_{acc}$ , stability tolerance  $\varepsilon_{stab}$ , selection criterion  $\eta_i$

- 1:  $V_0 \leftarrow \emptyset, \Lambda_0 \leftarrow \emptyset, s_0 \leftarrow 0, i \leftarrow 0, P_0 \leftarrow \infty$
- 2: **while**  $i \leq n_{max}$  **and**  $\max |y_N - \Lambda_N(s_i)| > \varepsilon_{acc}$  **and**  $P_i > \varepsilon_{stab}$  **do**
- 3:    $i \leftarrow i + 1$
- 4:    $\lambda_i \leftarrow \arg \max_{\lambda \in \Lambda_N} \eta_i(\lambda)$
- 5:    $P_i \leftarrow P_{\Lambda_{i-1}}(\lambda_i)$
- 6:    $v_i \leftarrow \frac{v_{\lambda_i} - \Pi_{V_{i-1}} v_{\lambda_i}}{P_i}$
- 7:    $\Lambda_i \leftarrow \Lambda_{i-1} \cup \{\lambda_i\}$
- 8:    $V_i \leftarrow V_{i-1} + \text{span}(v_i)$
- 9:    $s_i \leftarrow \text{GeneralizedKernelInterpol}(k, \Lambda_i, y_N(\Lambda_i))$
- 10: **end while**
- 11:  $n \leftarrow i, s_n \leftarrow s_i, \Lambda_n \leftarrow \Lambda_i$
- 12: **return** Iteration number  $n$ , approximant  $s_n$ , selected functionals  $\Lambda_n$

---

to be understood as suitable subvector extraction. These extension steps are iterated until any of the stopping criteria is satisfied.

In the algorithm, the use of the power function as a normalizing factor can be observed. If the power function value is too small, this normalization can become too inaccurate. Therefore the power function values are used as an additional stopping criterion for preventing instability.

The overall selection criterion that we apply is

$$\eta_i(\lambda) := w(\lambda) |\lambda(e_{i-1})|^\beta P_{\Lambda_{i-1}}(\lambda)^{1-\beta}, \quad (5)$$

which depends on the current approximation error  $e_{i-1}$ , the current generalized power function  $P_{\Lambda_{i-1}}$ , a parameter  $\beta \in [0, \infty]$  and a factor  $w(\lambda)$ . We motivate the latter two ingredients: As the operators  $L$  and  $B$  in general do not coincide in their differential order, different powers of the shape parameter  $\varepsilon$  appear in the corresponding matrix sub-blocks, which especially result in potentially large variations in the magnitude of the diagonal values. Therefore, we introduce additional weighting factors  $w(\lambda)$  for each functional by which their importance can be adjusted. For instance, it is typically important to ensure that sufficiently many Dirichlet functionals are chosen to ensure the correct values in those points and not only select interior differential functionals.

Further, as has been done in standard greedy kernel interpolation [47], a parameter  $\beta \in [0, \infty]$  is included in the selection scheme, which allows to balance the importance of the RHS data functions. Specifically the value  $\beta = 0$  is agnostic of the RHS functions as it only is based on the power function. Hereby it provides functionals that are good for all possible right hand sides, but certainly provides suboptimal selection if only a single BVP with a specific set of RHS data functions needs to be solved. In contrast, for “target-dependency”, adaptivity to the RHS data functions can be turned on by increasing  $\beta > 0$ , especially covering the analogues of the  $f$ -greedy ( $\beta = 1$ ),  $f \cdot P$  ( $\beta = 1/2$ ) and  $f/P$ -greedy ( $\beta = \infty$ ) procedures of function interpolation. Using this indicator, we conclude from the algorithm that, as long as the loop is continued – i.e., the accuracy threshold is not satisfied – there exists a functional for which an interpolation

error occurs, hence  $\eta_i(\lambda) > 0$  for at least one functional. A reasonable property of the selection criterion now is that  $\eta_i(\lambda_j) = 0$  for all  $j = 1, \dots, i - 1$  as the (generalized) interpolation conditions are met at the selected functionals. This guarantees that no previously selected functional is chosen twice.

As the  $\beta$ -greedy indicator and the iterative approximation scheme do not require the full kernel matrix, the overall scheme is very efficient. In linear algebra terms it corresponds to a partial pivoted Cholesky decomposition of the system matrix without assembling it in full, but only iteratively computing single rows. The power function values  $P_i$  of step 5 in Alg. 1 are the diagonal elements of the Cholesky factor, further explaining their role in controlling the stability of the algorithm. The pivoting rule is not one of the typical criteria used in numerical linear algebra but exactly corresponds to the  $\beta$ -greedy criterion, except for  $\beta = 0$ , which corresponds to a classical full pivoting. The Gram-Schmidt orthonormalization that is performed inside the algorithm generates an orthonormal basis of  $V_n$  that is the generalization of the so called Newton-basis in kernel interpolation. Especially the incremental approximants can be efficiently updated, as the previous coefficient vector can be reused and only a single new coefficient for the new basis vector needs to be computed for the generalized interpolation.

Overall, the training complexity is then  $\mathcal{O}(Nn^2)$ , i.e. only linear in  $N$ , hence allowing  $N$  in the order of millions on a standard PC. The prediction complexity at one point is only linear  $\mathcal{O}(n)$ , hence very fast when assuming a small expansion size  $n$ .

The overall greedy generalized kernel interpolation method using the selection indicator (5) is denoted as generalized  $\beta$ -greedy method. If  $\Lambda$  is given by point evaluations from PDE BVPs, we denote the approach as PDE- $\beta$ -greedy method.

**Remark 1** (Interpretation as Abstract Plain Kernel Interpolation). *If the generalized kernel interpolation procedure is well-posed, especially uniqueness for given RHS functions holds, then the generalized kernel interpolation procedure can be shown to be equivalent to a standard plain kernel interpolation problem on the set  $\Lambda$  using the functional kernel  $k_\Lambda(\lambda, \lambda') := \langle v_\lambda, v_{\lambda'} \rangle$ . Moreover, since an equivalence of the corresponding power functions can also be shown, the corresponding generalized  $\beta$ -greedy method corresponds to an abstract plain  $\beta$ -greedy interpolation procedure. For details, we refer to [17]. The relevance of this correspondence is that plain  $\beta$ -greedy kernel interpolation code can be reused for approximating BVP by just replacing the involved kernel.*

**Remark 2** (Relation to GEIM Method). *The generalized empirical interpolation method (GEIM) [26] on first sight may seem similar to greedy generalized interpolation, as it also is based on selecting functionals for providing approximants. In general, however, the setting is rather different: The GEIM aims at approximating any function from a given set  $F$  of functions rather than approximating a single target function. Also the selected basis functions in GEIM are functions from the target set instead of Riesz-representers of functionals. However, there is a special artificial situation where the methods become comparable: If the target set is  $F = \{k(x, \cdot) \mid x \in \Omega\}$  for a positive definite RBF kernel and the functionals are merely point evaluations, then the functionals selected by the generalized  $P$ -greedy method have Riesz-representers which are elements from  $F$  and exactly correspond to the basis chosen by the GEIM method.*



This equivalence transfers to the PDE-P-greedy procedure, if the abstract kernel  $k_\Lambda(\lambda, \lambda') := \langle v_\lambda, v_{\lambda'} \rangle$  can be written as radial kernel depending on the distance of the sampling points corresponding to  $\lambda$  and  $\lambda'$ . Indeed, the fact that  $k_\Lambda$  is radial ensures that it is uniquely maximized at  $\lambda = \lambda'$ . For other values than  $\beta = 0$  there cannot be an equivalence to GEIM, as the (PDE-) $\beta$ -greedy methods for  $\beta > 0$  provide adaptivity to each single given target function.

## 2.5 Convergence Rates

For the case of finite smoothness of the target function, i.e. assuming a kernel  $k$  for which the RKHS  $\mathcal{H}_k(\bar{\Omega})$  is norm-equivalent to some Sobolev-space, algebraic convergence rate results can be obtained. First, for the case of second order elliptic BVP functional evaluations we state a simplified (but coarser) bound that can be obtained from [48, Thm 5.1]. Especially we modify the index range and upper bound a residual term as presented in the proof in the appendix.

**Proposition 3** (Algebraic Convergence for BVP Residuals). *Assume  $k$  is a kernel on  $\bar{\Omega} \subset \mathbb{R}^d$  such that  $\mathcal{H}_k(\bar{\Omega}) \asymp H^\tau(\bar{\Omega})$ ,  $\tau > d/2 + 2$ . If  $u \in \mathcal{H}_k(\bar{\Omega})$ , then any PDE- $\beta$ -greedy scheme for  $\beta \in [0, 1]$  with uniform weighting  $w(\lambda) = 1$  provides an approximation sequence  $s_n$  such that for  $n \geq 6$  and abbreviating  $\alpha := (\tau - 2)/d - 1/2 > 0$  it holds*

$$\min_{i=1, \dots, n} \sup_{\lambda \in \Lambda} |\lambda(u - s_i)| \leq C n^{-\beta/2} n^{-\alpha} \log(n)^\alpha \|u\|_{\mathcal{H}_k(\bar{\Omega})}. \quad (6)$$

Analogously to Thm. 5.1 in [48], applying the well-posedness bound for the BVP problem (1) directly yields the same rate for the error in the  $L^\infty$  norm with a modified constant.

**Corollary 4** (Algebraic Convergence Rate for the  $L^\infty$ -Error). *Under the assumptions (and especially the constant  $C$ ) of Prop. 3 we have*

$$\min_{i=1, \dots, n} \|u - s_i\|_{L^\infty(\bar{\Omega})} \leq C \max(C_L, C_B) n^{-\beta/2} n^{-\alpha} \log(n)^\alpha \|u\|_{\mathcal{H}_k(\bar{\Omega})}. \quad (7)$$

Note that similar statements can be formulated for  $\beta \in (1, \infty]$ , cf. [48]. The striking feature of such bounds is that the  $n^{-\beta/2}$  factor is independent of the dimension and especially indicating that  $\beta > 0$ , i.e. schemes that involve the target values for functional selection have a better convergence rate than the case  $\beta = 0$ , which is agnostic of the RHS functions  $f, g$ .

For the case of infinitely smooth kernel and solution, exponential convergence can be proven, cf. Thm. 3.18 in [41], which we slightly simplify similarly to Prop. 3, as presented in the proof in the appendix.

**Proposition 5** (Exponential Convergence for BVP Residual). *Let  $k$  be the Gaussian kernel on a polygonal  $\bar{\Omega} \subset \mathbb{R}^d$  and  $\beta = 1$ . If  $u \in \mathcal{H}_k(\bar{\Omega})$ , then the PDE- $\beta$ -greedy scheme with uniform weighting  $w(\lambda) = 1$  provides an approximation sequence  $s_n$  such that for  $n \geq 6$*

$$\min_{i=1, \dots, n} \sup_{\lambda \in \Lambda} |\lambda(u - s_i)| \leq C n^{-\beta/2} e^{-c_1 n^{\frac{1}{2d}}} \|u\|_{\mathcal{H}_k(\bar{\Omega})}. \quad (8)$$

Again, using the BVP well-posedness estimate (1) we conclude the same exponential rate but with modified constants for the  $L^\infty$ -error, which is a simplification of Cor. 3.19 in [41].

**Corollary 6** (Exponential Convergence for  $L^\infty$ -Error). *Under the assumptions (and especially the constant  $C$ ) of Prop. 5 we have*

$$\min_{i=1,\dots,n} \|u - s_i\|_{L^\infty(\bar{\Omega})} \leq C \max(C_L, C_B) n^{-\beta/2} e^{-c_1 n^{\frac{1}{2d}}} \|u\|_{\mathcal{H}_k(\bar{\Omega})}. \quad (9)$$

We want to emphasize here a clear and striking advantage of these results over neural networks: These convergence rates are not only expression rates (i.e. existence statement for corresponding approximant with specified accuracy), but as well constructive, i.e. after the stated number of iterations a corresponding approximant is guaranteed to be computed by the greedy strategy. For neural networks, however, in general no guarantees can be given that the optimization procedure actually finds a suitable approximant in a limited number of iterations.

We further want to relate to convergence statements on Gaussian-Process based PDE-approximation [4] which states algebraic convergence in the so called fill-distance  $h_X$  of the points used for collocation. Hence there is only a convergence guarantee if the collocation points get dense in  $\Omega$ . In contrast, the  $\beta$ -greedy approximation can provide convergence statements only in terms of the expansion size  $n$  and avoiding the fill-distance, hence these results do not require that the points get dense everywhere in  $\Omega$ . This is considered to be an conceptual advantage of the greedy approach.

### 3 Extension to the Parametric Case

We now formulate the parametric extension of the problem to be considered and the approximation technique. We assume to have a bounded parameter set  $\mathcal{P} \subset \mathbb{R}^{d_\mu}$  and a possibly parametrized geometry, i.e. for all  $\mu \in \mathcal{P}$  we have an (open) domain  $\Omega(\mu) \subset \mathbb{R}^{d_x}$  for the position variable  $x$ , and indicate its closure as  $\bar{\Omega}(\mu)$ . We set the dimension of the overall position-parameter domain as  $d := d_x + d_\mu$ . We define the set  $\mathbf{\Omega} := \{\mathbf{x} = (x, \mu) \in \mathbb{R}^d \mid \mu \in \mathcal{P}, x \in \Omega(\mu)\}$  for position-parameter tuples  $\mathbf{x} = (x, \mu)$ . As the differential operator only acts on the boundary points of  $\Omega(\mu)$  and not on the overall boundary of  $\mathbf{\Omega}$ , we define  $\partial\mathbf{\Omega} := \{(x, \mu) \in \mathbb{R}^d \mid x \in \partial\Omega(\mu), \mu \in \mathcal{P}\}$ . In the simplest case of  $\Omega(\mu) = \Omega$  being constant w.r.t.  $\mu$ , this boundary set corresponds to a cylinder mantle in the position-parameter domain. Subsequently we define the union of these sets as  $\bar{\mathbf{\Omega}} := \mathbf{\Omega} \cup \partial\mathbf{\Omega}$ . Observe that this is just a notation in analogy to the non-parametric case, and the sets are not necessarily the interior, boundary, and closure of a given set  $\mathbf{\Omega}$  (e.g. in the given example  $\partial\mathbf{\Omega}$  does not contain the cylinder top/bottom faces). In particular, this general formulation allows discrete parameter sets  $\mathcal{P}$  without assuming any common structure between the PDEs corresponding to different values of  $\mu$ .

We assume that for any  $\mu \in \mathcal{P}$  a corresponding parametric PDE BVP problem is given, i.e. find  $u(\cdot, \mu) \in C^2(\Omega(\mu)) \cap C^0(\bar{\Omega}(\mu))$  such that

$$L(\mu)(u(\cdot, \mu)) = f(\mu) \text{ in } \Omega(\mu), \text{ and } B(\mu)(u(\cdot, \mu)) = g(\mu) \text{ on } \partial\Omega(\mu).$$

Here  $L(\mu)$  is assumed to be a second order operator of the form

$$(L(\mu)u)(x) = \sum_{i,j=1}^{d_x} a_{ij}(x, \mu) \partial_{x_i} \partial_{x_j} u(x) + \sum_{i=1}^{d_x} b_i(x, \mu) \partial_{x_i} u(x) + c(x, \mu) u(x),$$

with coefficient functions  $a_{ij}, b_i, c : \Omega \rightarrow \mathbb{R}$ , and similarly for the boundary value operator  $B(\mu)$ . We assume that the problem is well-posed, i.e. for any  $\mu$  we assume the existence of a unique classical solution  $u(\cdot, \mu)$ . Thus, the parametric solution can be understood as a function  $u : \bar{\Omega} \rightarrow \mathbb{R}$ . Furthermore we suppose a certain regularity of the solution in the position and the parameter, i.e. we assume that  $u \in \mathcal{H}_k(\bar{\Omega})$  for some position-parameter kernel  $k : \bar{\Omega} \times \bar{\Omega} \rightarrow \mathbb{R}$ . For simplicity we restrict to product kernels, i.e.  $k(\mathbf{x}, \mathbf{x}') = k_x(x, x') \cdot k_\mu(\mu, \mu')$  for suitable position kernel  $k_x : \mathbb{R}^{d_x} \times \mathbb{R}^{d_x} \rightarrow \mathbb{R}$  and parameter kernel  $k_\mu : \mathbb{R}^{d_\mu} \times \mathbb{R}^{d_\mu} \rightarrow \mathbb{R}$ . Such product kernels correspond to tensor products of RKHSs and are very versatile [3, 1]. Then  $\mathcal{H}_k(\bar{\Omega})$  is a restriction of the tensor product space  $\mathcal{H}_{k_x}(\mathbb{R}^{d_x}) \otimes \mathcal{H}_{k_\mu}(\mathbb{R}^{d_\mu})$  to the domain  $\bar{\Omega}$ . The advantage of this structure is that the differential operator only acts on the position variable, for instance  $L(\mu)^{[1]}k(\mathbf{x}, \mathbf{x}') = (L(\mu)^{[1]}k_x(x, x')) \cdot k_\mu(\mu, \mu')$ . This simplifies the practical realization as generic and modular implementation and combination of the corresponding kernel functions is possible. E.g., different regularity assumptions w.r.t. the parameter and the position could be realized by choosing corresponding position and parameter kernels. Assuming that  $f, g$  and the coefficients  $a_{ij}, b_i, c$  are  $C^\infty$  with respect to the position variable and  $\partial\Omega(\mu)$  is a  $C^\infty$ -boundary, uniform ellipticity of  $L(\mu)$  and  $c \leq 0$  implies existence, uniqueness and that  $u(\cdot, \mu)$  is infinitely smooth with respect to the position variable. From the RB literature it is known that differentiability of coefficients w.r.t. the parameter transfers to corresponding differentiability of the solution with respect to the parameter [16]. But such smoothness in the solutions can occasionally as well be obtained despite less regular data or geometry. As an example we will consider a non-Lipschitz domain including topology change in the experiments.

The generalized interpolation setting can then directly be applied by identifying

$$\Lambda := \Lambda_L \cup \Lambda_B := \{\delta_x \circ L(\mu) \mid (x, \mu) \in \Omega\} \cup \{\delta_x \circ B(\mu) \mid (x, \mu) \in \partial\Omega\} \subset \mathcal{H}_k(\bar{\Omega})',$$

and applying the method from Sec. 2 using the position-parameter domain  $\bar{\Omega}$  instead of the position domain  $\bar{\Omega}$ . Especially the final approximant is  $s_n : \bar{\Omega} \rightarrow \mathbb{R}$ , which can be interpreted as a global a-priori surrogate model similar to PINNs [32], PGD [29], etc. The “offline-phase” consists of a single training phase of the model (sampling of the position-parameter domain and boundary, greedy search of collocation points and computation of approximant). The “online-phase” then simply consists of pointwise evaluation of the surrogate in any new position-parameter tuple  $\mathbf{x} \in \bar{\Omega}$ .

We want to explicitly state that we avoid a “standard approach” of parametric approximation, which would consist of providing some solutions (snapshots) for some fixed parameter samples. Then an overall parametric approximant would be obtained by some sort of parametric interpolation or other linear combination of these precomputed particular solutions. The reason for not following this approach is the overall solution expansion size, which would grow multiplicatively in the number of parameter samples used for the parametric interpolation (or more general linear combination) and the individual expansion size of each solution snapshot. We expect that by avoiding this tensor-product construction, greedy strategies over the parameter-state domain are able to place samples more intelligently and sparsely than choosing a fixed tensor-product grid.

We now want to briefly discuss the changes in the error analysis for the parametric extension. First, with respect to the position-parameter domain, the elliptic (w.r.t. position variable) differential operator is degenerate in the parametric direction as there are no parametric derivatives. So the framework of [48] might seem not fully suitable at first glance. However, when inspecting the proof of the convergence rates leading to Prop. 3 or Prop. 5, one realizes that actually no ellipticity assumption is required for the convergence rates of the functional residuals. Only for the conclusion of the  $L^\infty$ -error convergence rates of Cor. 4 and Cor. 6, a well-posedness result is required. If we assume uniform (in parameter) ellipticity of the differential operator and uniform (in parameter) boundedness of its coefficients and uniform boundedness of the RHS data functions, Eqn. (1) can be formulated with constants  $C_L, C_B$  which are independent of  $\mu \in \mathcal{P}$ . Then, especially, the bound (4) holds for the whole position-parameter domain, providing an upper bound for the error on single slices  $\Omega(\mu) \times \{\mu\}$ , hence for any  $\mu \in \mathcal{P}$  it holds

$$\begin{aligned} \|u(\cdot, \mu) - s_n(\cdot, \mu)\|_{L^\infty(\bar{\Omega}(\mu))} &\leq \|u - s_n\|_{L^\infty(\bar{\Omega})} \\ &\leq C_L \sup_{\lambda \in \Lambda_L} \lambda(u - s_n) + C_B \sup_{\lambda \in \Lambda_B} \lambda(u - s_n) \end{aligned} \quad (10)$$

Then, also convergence rates for the RHS transfer to convergence rates for the left hand side (LHS) restricted to slices.

## 4 Numerical Experiments

The following experiments were performed with MATLAB R2024b on a system with i7-1355U 1700 MHz CPU and 32 GB memory. For full reproducibility we provide the code<sup>1</sup>.

In all examples, we consider a standard Poisson problem with Dirichlet boundary values, i.e.  $L = -\Delta$ ,  $B = \text{Id}$ , hence we only need to specify the domains  $\mathcal{P}, \Omega(\mu)$  and the RHS data functions  $f(\cdot, \mu), g(\cdot, \mu)$  in the following model problems.

### 4.1 Nonaffine Geometry Parametrization

We start with an example of a non-affine geometry parametrization of “moving circles”, where the position-domain is  $\Omega(\mu) = B_1(0) \cup B_1((\mu, 0)^T) \subset \mathbb{R}^2$  for  $\mu \in [0, 1.1] =: \mathcal{P} \subset \mathbb{R}$ , hence  $d_x = 2, d_\mu = 1$  and the overall state dimension is  $d = 3$ . The parameter is chosen such that the topology of the geometry changes from a single connected to two disconnected circular components. The kinks in the domain boundary for  $\mu \in (0, 1)$  are such that the domain  $\Omega(\mu)$  is non-convex. Such a geometry parametrization is clearly non-affine and no fixed spatial point set can be chosen, and no standard RB or any parametric interpolation or linear combination of spatial “snapshot” solutions would be suitable as such would not exactly recover the boundary geometry.

The position-parameter domain  $\bar{\Omega}$  is consisting of the union of two (skew) cylinders and as training set of the functionals we sample randomly and uniformly  $N_L := 10^4$  interior and  $N_B := 10^4$  boundary points, hence  $N = N_L +$

<sup>1</sup><https://gitlab.mathematik.uni-stuttgart.de/pub/ians-anm/mu-pde-beta-greedy>.

$N_B = 2 \cdot 10^4$  sampling points, which determine the corresponding training set of functionals, by corresponding point evaluations of either the differential or boundary operator, and are visualized in Fig. 1a).

We consider two cases, first a case of a smooth solution, then a more challenging setting with a singular solution.

For the smooth solution case, we assume the known solution  $u(x, \mu) = \frac{1}{2}(\|x\|^2 + \mu^2)$  and choose  $f := Lu$ ,  $g := u|_{\partial\Omega}$  correspondingly. This allows us to assess true pointwise errors as quality criterion.

Anticipating the  $C^\infty$  regularity of the solution, we choose as kernel a product of Gaussian kernels for both the position and the parameter coordinate, but with different (squared) shape parameters  $\varepsilon_\mu^2, \varepsilon_x^2$ .

We choose an  $f$ -greedy strategy ( $\beta = 1$ ) as this seems most promising from the convergence rate analysis. We fix the maximum expansion size as  $n_{max} = 100$  and the stopping tolerances as  $\varepsilon_{acc} = \varepsilon_{stab} = 1 \cdot 10^{-15}$ . The functional weightings  $w(\lambda)$  are chosen as  $w_B \in \mathbb{R}_{>0}$  for  $\lambda \in \Lambda_B$  (to be selected later), and  $w_L = 1$  for  $\lambda \in \Lambda_L$ .

The (squared) shape parameters  $\varepsilon_x^2, \varepsilon_\mu^2$  and the functional weighting parameter  $w_B$  are dominantly influencing the prediction accuracy of the models, hence are considered to be hyper-parameters in this example. Therefore each of these parameters was consecutively selected by a 1D grid search over some discrete values of the parameter and choosing the parameter resulting in the least ‘‘loss’’ of the approximant measured over a randomly drawn validation set of 10000 interior  $\Lambda_{L, val}$  and 10000 boundary functionals  $\Lambda_{B, val}$ . As loss function for validation of a model function we choose a weighted sum of the maximum interior and maximum boundary BVP residual error

$$e_{val}(s_n) := \gamma_L \sup_{\lambda \in \Lambda_{L, val}} |\lambda(u - s_n)| + \gamma_B \sup_{\lambda \in \Lambda_{B, val}} |\lambda(u - s_n)|, \quad (11)$$

which is motivated by the RHS of the error equation (10). In lack of true values for the constants, we simply set  $\gamma_L = \gamma_B = 1$ . The final selected parameters are  $\varepsilon_x^2 = 0.0063096, \varepsilon_\mu^2 = 0.01, w_B = 1.0$ .

The greedily selected functionals (indicated by colors and their evaluation point location) are given in Fig. 1b), in which 38 interior and 35 boundary functionals were chosen. One can clearly see the sparsity compared to the full training set of functionals in subplot a). The greedy strategy seems to select the functionals in a well-distributed fashion. The training time for selecting the 73 functionals and computing the approximate solution was 0.32 seconds.

In Fig. 2 we illustrate the parametric approximate solution evaluated for several parameters. The changing topology is clearly visible. The resulting absolute accuracy of the model is  $\|u - s_n\|_{L^\infty(\bar{\Omega})} = 2.9719 \cdot 10^{-7}$  measured over an independently drawn test set in  $\bar{\Omega}$ .

In Fig. 3 we illustrate the training BVP residual decay, i.e.  $\max_{\lambda \in \Lambda_N} |\lambda(u - s_n)|$ . One can clearly see the overall asymptotic exponential convergence, which is what we expect in view of the error convergence analysis. But also, we recognize local non-monotonicity or plateaus, which is why the minimum in the LHS of the error bounds in Sec. 2.5 indeed is not an artifact but seems useful. For each curve, we also report the ratio  $r_{bnd}$  of selected boundary functionals over the total number of selected functionals, which is naturally increasing with growing  $w_B$ . Also, occasional early stopping of the greedy loop due to numerical

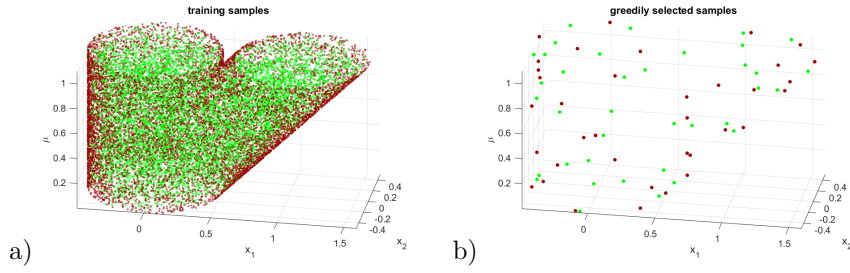


Figure 1: Functional samples for the moving circles example, indicated by point evaluation sites for the interior (green) and boundary operator (red). Subplot a) indicates the training samples. Subplot b) illustrates the greedily selected functionals for the smooth solution case for selected hyper-parameters.

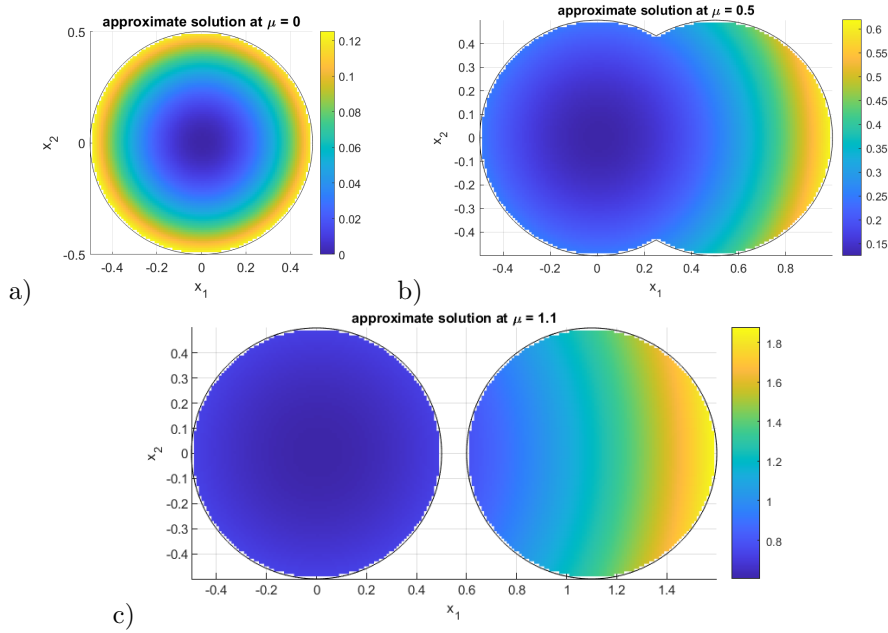


Figure 2: Visualization of the smooth solution case for the moving circles example: Approximate solution for selected hyper-parameters at  $\mu = 0.0, 0.5$  and  $1.1$ .

accuracy reasons can be observed. The  $L^\infty$ -errors of the final approximants are as well reported for each curve in the legend, and we note that indeed a local minimum is to be expected in the interval  $w_B \in [10^{-1}, 10^1]$ , which is consistent with the optimized value  $w_B = 1$  reported earlier.

For the singular solution case, we choose  $g(x, \mu) = 0$  and  $f(x, \mu) = -1$ . Despite the simple data functions, the geometrical parametrization results in a lack of an explicit closed form representation of the solution for the parameters  $\mu \in (0, 1)$ . For  $\mu = 0$  and  $\mu \in [1, 1.1]$  the solution  $u(\cdot, \mu)$  is expected to be  $C^\infty(\Omega(\mu))$  due to the smoothness of the data functions and the boundary  $\partial\Omega(\mu)$ .

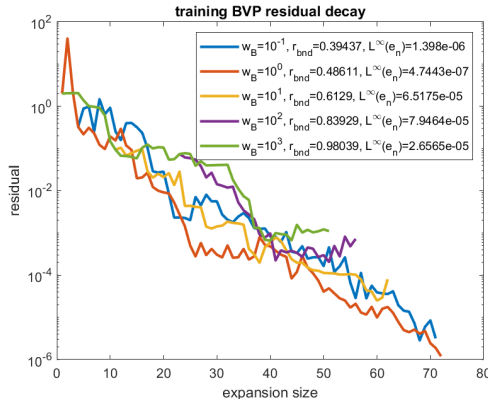


Figure 3: Visualization of BVP training residual convergence, ratio of selected boundary functionals (indicated as  $r_{bnd}$ ) and true  $L^\infty$ -error (indicated as  $L^\infty(e_n)$ ) at maximum expansion size for different boundary functional weighting values  $w_B \in \{10^{-1}, \dots, 10^3\}$  for the moving circles example with the smooth solution case.

But for  $\mu \in (0, 1)$  it is expected to have singularities in its derivatives due to the entering corner. Due to this anticipated reduced regularity now the quadratic Matérn kernel (2) is chosen. Still, this clearly is an example where the target function  $u$  is outside the RKHS  $\mathcal{H}_k(\bar{\Omega})$ , hence we do not expect the convergence rates as specified in Sec. 2.5 and actually the convergence is theoretically unclear at all. But still the example is interesting to assess. We cannot access the true error of the approximants, but can only refer to the BVP functional residual values.

Instead of  $f$ -greedy we turn to the  $P$ -greedy ( $\beta = 0$ ) strategy, as the target-data dependent criteria tend to cluster points and imply early instability in the case of target functions outside the RKHS. In contrast, the  $P$ -greedy strategy is known to produce more uniformly distributed points [46]. We fix the maximum expansion size as  $n_{max} = 1000$  and the stopping tolerances as before to  $\varepsilon_{acc} = \varepsilon_{stab} = 1 \cdot 10^{-15}$ . The shape parameters were manually chosen as  $\varepsilon_x = \varepsilon_\mu = 3$  and the functional weightings as  $w_B = 100000^{1/2}$  and  $w_L = 1$ .

In Fig. 4a) we illustrate the selected 876 interior and 124 boundary functionals. The uniformity and the considerably larger number of functionals compared to the smooth example are evident. The training for selecting the 1000 functionals took 9.35 seconds. This is approximately a factor 8 less than we would expect from a pure  $n^2$  scaling compared to the runtime in the smooth example. We report the cumulative number of boundary and interior functionals during the greedy selection in Fig. 4b). The resulting maximum greedy selection criterion over the iterations is plotted in Fig. 4c). We nicely see a monotonic decay over almost two orders of magnitude. We can recognize two phases, where first only boundary functionals are chosen, then dominantly the interior is being sampled. This is reflected in the selection criterion (i.e. weighted power function) decay in different decay regimes. The phase of predominantly boundary functional selection for  $n$  up to 100 corresponds to the pure (non PDE) func-

tion approximation of the infinitely smooth zero-boundary value function in an effective  $d - 1$  dimensional manifold with correspondingly expected more rapid decay. When approximating the interior domain starting at about  $n > 100$ , the decay rate is reduced due to the higher degree of the differential operator, the full dimension  $d_x$  of  $\Omega(\mu)$  and the lower regularity of the target function. The merely algebraic decay is very clearly visible.

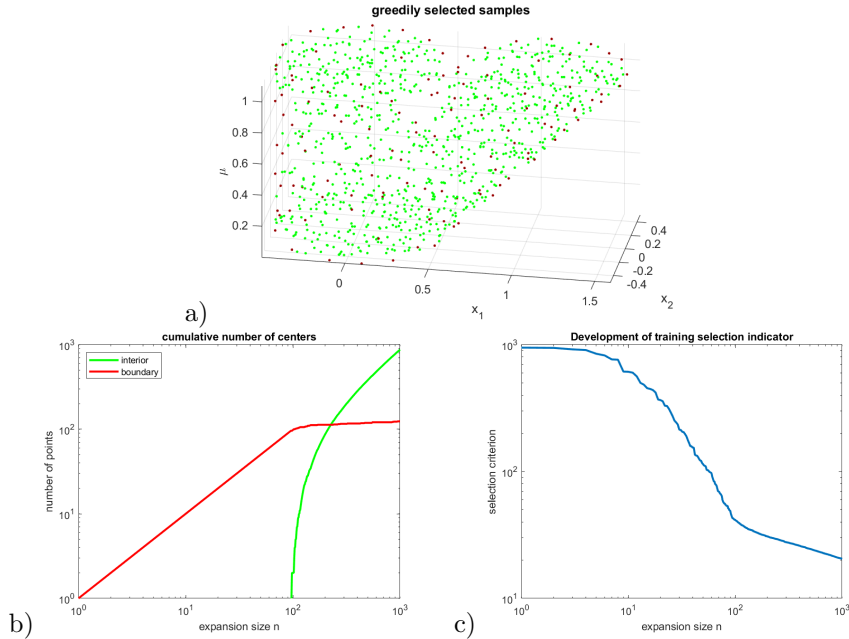


Figure 4: a) Greedily selected functional samples for the moving circles example with the nonsmooth solution case, indicated by point evaluation sites for the differential (green) and boundary operator (red). b) Cumulative number of boundary and interior functionals during greedy selection. c) Decay of the greedy selection indicator during training.

However, the difficulty of the given example is reflected by several observations. In Fig. 5 we illustrate the parametric approximate solution evaluated for several parameters. As we have no closed form solution of the problem, we do not give absolute error quantification. But qualitatively the solution seems reasonable in the sense that the boundary values are visually accurately captured, and quantitatively realize a maximum absolute value over the boundary training points of 0.00868. Also the sign of the solution is consistent with the (negative) source function. Due to the nonsymmetric point/functional placement, the pure expected rotational symmetry of the solution for  $\mu = 0$  and  $\mu = 1.1$  is slightly distorted in the approximation.

Next we investigate the corresponding BVP functional residuals, by plotting the absolute value of the interior residuals  $|\lambda(u - s_n)|$  for  $\lambda \in \Lambda_L$  in Fig. 6 for the same parameter values as before. We observe that there are regions of considerably large absolute residual value. But as well in large regions we observe nicely low residuals. The problems particularly seem to persist in the regions



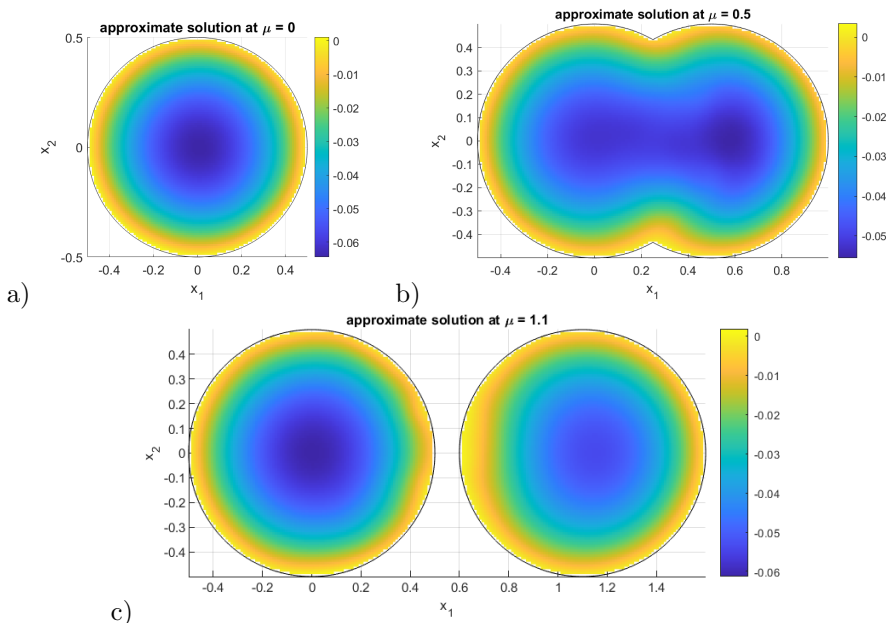


Figure 5: Visualization of the nonsmooth solution case for the moving circles example, approximate solution at  $\mu = 0, 0.5$  and  $1.1$ .

of the entering corner. So overall for this nonsmooth example we conclude that while we do not guarantee any theoretical approximation quality, we are able to provide some reasonable approximation.

## 4.2 Moving Source Term

The next example is aiming at a moving structure underlying the problem. Moving structures are typically difficult for RB methods, as this requires additional (empirical) interpolation steps for the data functions and the solution manifolds may have slowly decaying Kolmogorov  $n$ -widths. We choose the position domain to be the parameter-independent unit-square  $\Omega(\mu) := \Omega := (0, 1)^2$  for all  $\mu \in \mathcal{P} := [0, 1]$ , hence  $d = d_x + d_\mu = 2 + 1 = 3$ . We define the parametric source function to be a cut-off inverted parabola  $f(x, \mu) = 50 \max(1 - \frac{1}{16} \|x - m(\mu)\|^2, 0)$  with parametric midpoint  $m(\mu) := (\frac{1}{10} + \frac{4}{5}\mu)(1, 1)^T \in \Omega$ . This source function is non-affinely parameter dependent, i.e. it is not a linear combination of parameter-independent functions with parameter-dependent coefficients. The source function for the parameters  $\mu \in \{0.0, 0.5, 1.0\}$  is visualized in Fig. 7a). This clearly motivates the notion “moving source” as the source function has a local support, which is a circle with the given midpoint being translated. The Dirichlet values are set to homogeneous  $g = 0$  for all  $(x, \mu) \in \partial\Omega$ .

Due to the non-differentiability of  $f$  at the boundary of its support, and the non-differentiable boundary, we cannot expect more than twice differentiability of the solution in the interior of  $\Omega$ . Therefore, we again choose the quadratic Matérn kernel for the position and the parameter coordinate with shape parameters  $\varepsilon_x$  and  $\varepsilon_\mu$ . The RKHS of this kernel matches this anticipated regularity

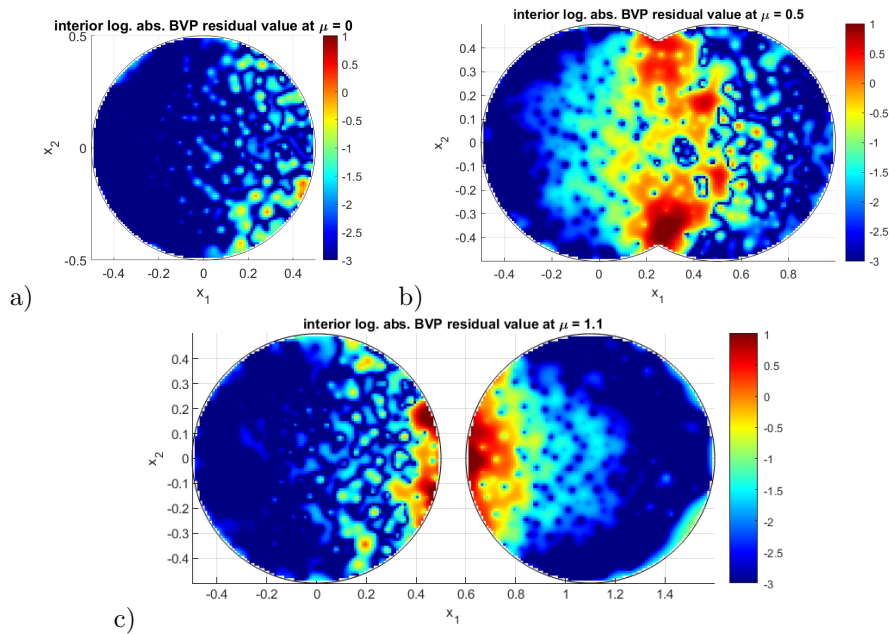


Figure 6: Visualization of interior residuals in case of the nonsmooth solution for the moving circles example at  $\mu = 0.0, 0.5$  and  $1.1$ .

in the interior.

Again, we sample randomly and uniformly  $N = N_L + N_B = 10^4 + 10^4$  evaluation points, which correspond to the training functionals as visualized in Fig. 8a). We choose the  $f$ -greedy strategy with maximum expansion size  $n_{max} = 2000$  and the same accuracy and stability tolerances and functional weighting  $w_L$  as before.

The two shape parameters and the functional weighting  $w_B$  are again hyperparameters and were selected by minimizing the loss term of (11) by 3 consecutive 1D grid-searches. In this example the default loss weights resulted in a model with too few boundary functional selections, therefore we reduced the interior weight to  $\gamma_L = 0.005$ . The resulting parameters are  $\varepsilon_x = 5.0, \varepsilon_\mu = 15.8114, w_B = 1000$ .

The approximate solutions for some parameters are visualized in Fig. 7b). The symmetry of the problem with respect to the position-diagonal is clearly visible. The selected functionals consisting of 1592 interior and 408 boundary functionals are given in Fig. 8b). Note the clear clustering of the selected functionals around the diagonal of the cube, which corresponds to the region where the source is nonzero. The training of the model with these optimized parameters took 42.03 sec, which indeed is close to a factor 4 increase compared to the former experiment with an  $n = 1000$  expansion, hence is consistent to the expected  $n^2$  scaling.

The decay of the maximum BVP residual is plotted in Fig. 8d), which again indicates an overall rate which seems algebraic, but again shows clear non-monotonicity. The cumulative number of selected interior and boundary functionals is shown in Fig. 8c). Again, we observe different phases: The initial

plateau of up to  $n = 50$  is caused by the choice of mostly boundary functionals due to the large value of  $w_B$ . The BVP functional error only decays adequately as soon as a larger number of interior functionals have been chosen.

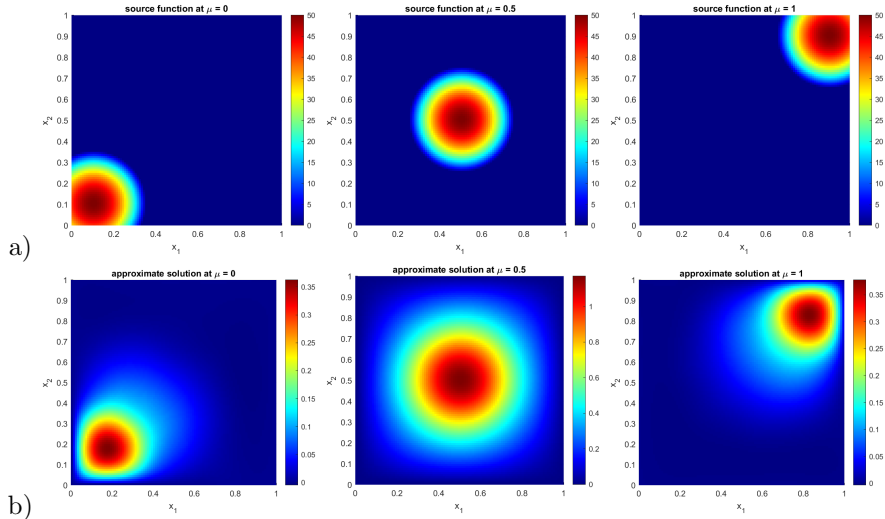


Figure 7: a) Visualization of the moving source functions for parameters  $\mu = 0.0, 0.5, 1.0$ . b) Plot of the corresponding approximate solution.

In order to obtain more quantitative error statements, we evaluate the  $L^\infty(\Omega_x)$ -error compared to a reference solution obtained by a FEM. For this we choose a uniform triangular mesh with 20000 elements and P1 ansatz functions. In addition to the PDE- $f$ -greedy procedure ( $\beta = 1$ ) we now also include the  $\beta = 0.75, 0.5$  and  $\beta = 0$  cases. Also, we consider a full kernel collocation and a coarser FEM approximation as methods for comparison. For a random position-parameter test set, all parameter components in the test vectors would differ and require a separate fine FEM solve for each of those parameter values, which would clearly be computationally infeasible. Instead, we construct a structured Cartesian product test set based on choosing  $n_\mu = 20$  equidistant parameter values  $\mathcal{P}_h \subset \mathcal{P}$  and  $n_x = 101^2$  position samples as the vertices  $\Omega_h \subset \Omega$  of the fine reference FEM mesh. Table 1 lists the resulting parameters and errors.

To make the FEM and PDE- $\beta$ -greedy approaches comparable we choose models with similar number of degrees of freedom (DOFs), where the number of DOFs for a nonparametric FEM solution are simply multiplied by the number of parameter samples, as this is the amount of coefficients that must be stored to represent the  $n_\mu$  parametric solutions. Therefor we consider an equidistant  $10 \times 10$  nodes FEM mesh on the unit square and choose the 20 parameter samples, as this results in 2000 degrees of freedom for those 20 FEM solutions. For the full kernel collocation approach, only the kernel parameters were selected by validation, the ratio of boundary value points was fixed a priori. We can observe that all the greedy procedures with  $\beta > 0$  are clearly superior over the full collocation approach, which is not surprising as the latter uses a fixed non-adapted center set, while they are better but comparable for  $\beta = 0$ , which

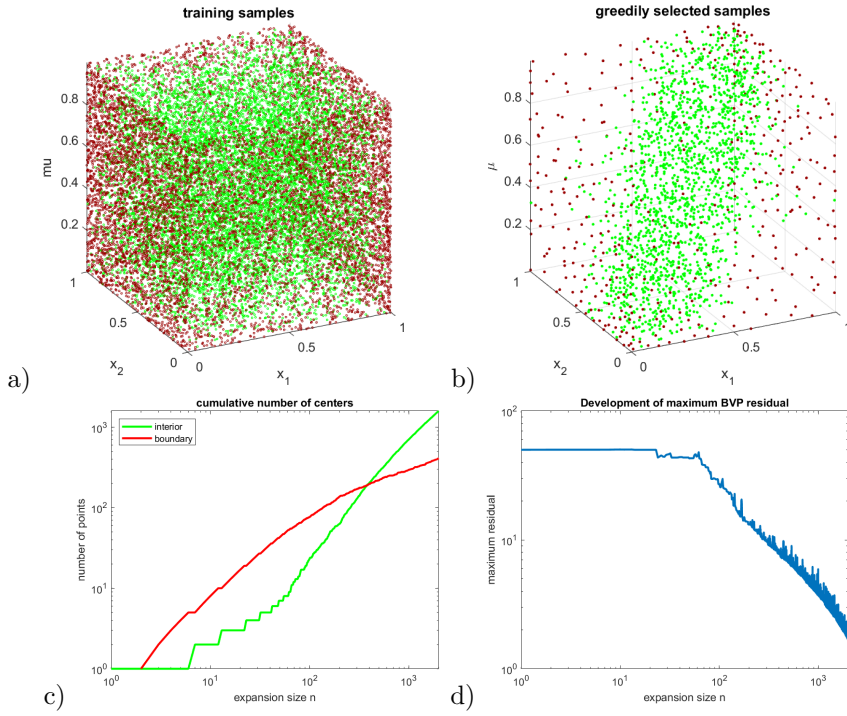


Figure 8: a) Training functionals, indicated by the point evaluation sites for the differential (green) and boundary operator (red) for the moving source example. b) Subset of greedily selected functional samples. c) Cumulative number of selected boundary and interior functionals. d) Decay of the maximum training BVP residual absolute value over the iterations.

PDE- $\beta$ -greedy						
$\beta$	$n$	$\varepsilon_x$	$\varepsilon_\mu$	$w_B$	$r_{bnd}$	$L^\infty$ -error
0	2000	5	5	100	0.2825	0.17416
0.5	2000	5	15.8114	200	0.2795	0.032093
0.75	2000	5	15.8114	100	0.1135	0.027812
1	2000	5	15.8114	1000	0.204	0.032785
Full collocation						
	$n$	$\varepsilon_x$	$\varepsilon_\mu$		$r_{bnd}$	$L^\infty$ -error
	2000	5	5		0.1	0.21286
FEM						
$n_x$	$n = n_\mu \cdot n_x$					$L^\infty$ -error
100	2000					0.088282

Table 1: Resulting selected parameters and  $L^\infty$ -errors for different PDE- $\beta$ -greedy variants: Full collocation and FEM for the moving source example.

still selects the centers from a larger set. In comparison to the FEM approach, we can recognize that the target function-dependent greedy selection criteria result in models with clearly lower error than the FEM approximation with

comparable number of DOFs, even if it is not a large factor of improvement. So the function adaptivity pays off. Note that the FEM error is to be understood as being optimistic for the FEM method, as for a full parametric assessment, some parametric interpolation, etc. would need to be included, which cannot decrease the FEM errors for the snapshot solutions but will presumably yield larger values for intermediate parameter values. Especially this FEM error is a lower bound for any parametric MOR method that is based on those 20 parametric FEM solution snapshots and has a reproduction property, e.g. parametric interpolation, Galerkin-projection, etc.

### 4.3 High-dimensional Domains

To investigate the possibilities of the scheme for high-dimensional cases we consider as positional domain the non-parametric unit-hypercube  $\Omega := (0, 1)^{d_x}$ ,  $d_x \in \{2, \dots, 9\}$  with single scalar parameter  $\mu \in [0, 1]$ , hence  $d_\mu = 1$  and overall dimension  $d \in \{3, \dots, 10\}$ . We consider a model that can easily be generalized to arbitrary input dimension by prescribing as known solution a sinus wave  $u(x, \mu) := \sin(\langle x, \kappa(\mu) \rangle)$  with parametrized frequency

$$\kappa(\mu) = \frac{1}{d_x}((1 - \mu)\kappa_0 + \mu\kappa_1)(1, \dots, 1)^T \in \mathbb{R}^{d_x},$$

with  $\kappa_0 := \pi$  and  $\kappa_1 := 2\pi$  such that  $\mu = 1$  always results in a complete sinus period and  $\mu = 0$  in half a period along the diagonal of the hypercube independently of  $d_x$ . The RHS functions  $f$  and  $g$  are chosen correspondingly. This again allows us to assess the true pointwise errors of the approximation to the exact solution. To cover higher dimensions more accurately we raise the number of training samples of functionals to  $N_L := N_B := 10^5$ , hence  $N = 2 \cdot 10^5$ .

In view of the  $C^\infty$  regularity of the solution, as before we use the product of a position and parameter Gaussian kernel.

We use an  $f$ -greedy criterion and fix the maximum expansion size to  $n_{max} = 1000$  and the stopping tolerances as before. The functional weightings were set to  $w_L := 1$  and  $w_B := 100$ .

For comparability over the dimensions, we do not do a meta-search of parameters. Instead we set  $\varepsilon_x^2 := 5.0/d_x$ ,  $\varepsilon_\mu^2 := 2.5$  which yields reasonable but certainly improvable results in all considered dimensions. As the diagonal of the unit-cube  $\Omega$  scales with  $\sqrt{d_x}$ , the specified choice of  $\varepsilon_x$  results in “equal” kernel decay along the diagonal in all dimensions. We refer to this as “isotropic Gaussian” in the following. Note that a sufficiently fast decaying choice of dimension-dependent shape parameters is also the key for obtaining dimension-independent constants in worst-case error bounds [13].

In Fig. 9 we illustrate the parametric approximate solution evaluated for two extreme parameters a)  $\mu = 0$  and b)  $\mu = 1$  for the  $d_x = 2$  case. The doubling in frequency along the diagonal is clearly visible. The accurate capturing of the diagonal symmetry even with an isotropic kernel can be verified.

In order to illustrate the  $L^\infty$  convergence rates, we evaluated the error measured over  $n_{L,test} + n_{B,test} = 10000 + 10000$  test functionals for increasing model sizes sampled at 13 (approximately) logarithmically equally distant model sizes  $n = 10, \dots, 1000$ . The resulting errors for the different dimensions are plotted in Fig. 10a). For every dimension we clearly recognize an exponential decay in

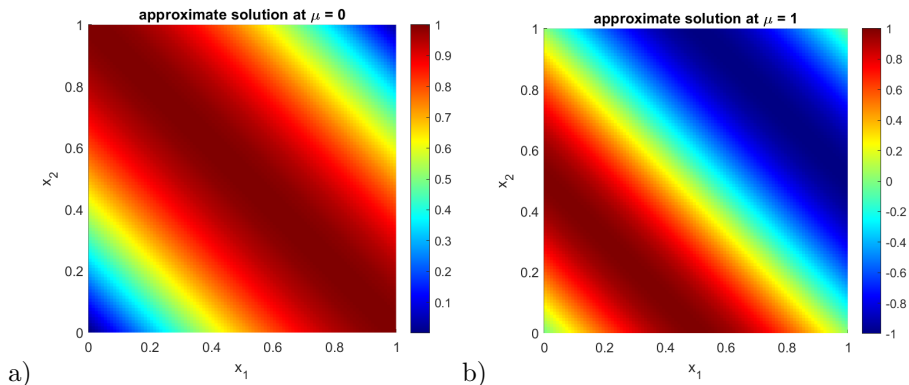


Figure 9: Visualization of sinus-source example approximate solution in  $\mathbb{R}^{d_x}$  for  $d_x = 2$  a) at  $\mu = 0$  and b) at  $\mu = 1$ .

the log-log plot. With increasing space dimension it is more difficult to provide small approximation errors, which is reflected by the slower decay.

In the given example, the radial kernel obviously is not adapted to the solution structure. As final experiment, we want to illustrate how problem-adapted kernels can lead to considerable improvements.

Using strong prior knowledge about the translation-invariance of the solution, we want to reflect this with an anisotropic kernel choice for the position variable. For this, we choose a suitable matrix  $B$  in (3) by splitting the position space into  $v_1 := \frac{1}{\sqrt{d_x}}(1, \dots, 1)^T \in \mathbb{R}^{d_x}$  and an orthogonal complement, i.e.  $v_2, \dots, v_{d_x} \perp v_1$  being pairwise orthogonal and normalized  $\|v_i\| = 1$ . Then we obtain the orthogonal matrix  $V := [v_1, \dots, v_{d_x}] \in \mathbb{R}^{d_x \times d_x}$  and set

$$B := V \begin{pmatrix} 5.0/d_x & 0 \\ 0 & 0.0025 \cdot I_{(d_x-1) \times (d_x-1)} \end{pmatrix} V^T.$$

The parameter kernel is chosen as before as standard Gaussian with  $\varepsilon_\mu^2 = 2.5$ .

The resulting  $L^\infty$ -error convergence curves are given in Fig. 10b). Compared to plot Fig. 10a), we indeed see a considerable improvement in approximation, which even seems to be partially dimension-independent until certain model sizes are reached.

We want to comment that the assumption of knowing the most important direction of variation, i.e.  $v_1$  can be relaxed. By applying an active subspace detection procedure [8], i.e. sampling the source function gradient at the training points and computing  $v_1$  as the principal component, an active subspace for  $f$  can be identified. When using this numerically identified subspace  $v_1$  in the anisotropic kernel, the resulting  $L^\infty$ -errors only change marginally in the present example. A reason for the success of this procedure may be that in our case due to the isotropy of the differential operator the active subspace from the source function transfers to the active subspace of the solution.

These results – even if not being meta-parameter-optimized – indicate promising approximation properties for high-dimensional examples.

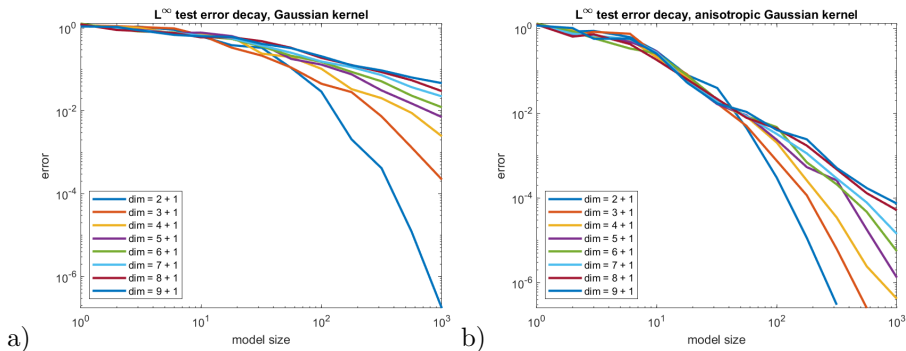


Figure 10: Test  $L^\infty$ -error convergence for the high-dimensional sinus-source example with varying position-dimensions and using a) an isotropic Gaussian kernel and b) an anisotropic Gaussian kernel.

## 5 Summary and Conclusion

In the present article we extend the scale of  $\beta$ -greedy schemes for PDE approximation to the parametric case by the use of position-parameter kernels. The procedure is easily implemented as a greedy kernel interpolation scheme using an abstract kernel on BVP evaluation functionals. Correspondingly the method inherits computational advantages such as linear training complexity in the overall number of candidate collocation centers and only quadratic complexity in the final kernel expansion size. Analytical convergence statements suggest that one can expect exponential convergence rates, hence very efficient and sparse expansions, in the case of smooth solutions and smooth kernel. Especially for  $\beta > 0$  an additional dimension-independent decay factor appears suggesting that RHS-adaptive center selection is indeed provably preferable over selection schemes that are agnostic of the special source/boundary values. The exponential convergence rates were experimentally verified in different scenarios. We do not suggest the present approach as a competitor to standard RB methods for parameter separable low space-dimensional elliptic cases, where RB-methods are known to provide exponential convergence rates. Rather we demonstrated that the present PDE- $\beta$ -greedy approach can be beneficial in cases that cover nontrivial geometry parametrization including topology changes, moving structures or high-dimensional state domains. We do not require explicit parametric geometry transformations of the domain as long as we can sample points from the interior and the boundary to generate the candidate collocation point sets.

Beside those positive insights, limitations of the procedure appear in cases, e.g. with singular solutions. This is due to the fact that we aim for strong solutions, hence assume classical regularity. Problems with solutions that have corner singularities, cannot be approximated well with the presented schemes. Still some limited approximation is possible, cf. the singular solution case of Sec. 4.1 and the numerical comparison to FEM approximation in [48].

As interesting outlook we see experimental investigation for more general non-elliptic PDEs, e.g. advection or wave-equation problems. These also pose problems for linear subspace-based MOR, as they face slowly decaying Kol-

mogorov  $n$ -widths [15, 31] when relying on separating the spatial and time coordinate and aiming for a spatial approximation space that is used for the whole time axis. In contrast, the current kernel-greedy schemes would circumvent this problem by inherently constructing efficient approximation spaces in the time-space domain. This will be addressed in more detail in future work.

A further immediate direction for extension is the treatment of nonlinear PDEs by iterative linearizations and corresponding fixpoint schemes. This would then enable efficient solution of problems in high-dimensions such as kinetic equations, optimal control (Hamilton-Jacobi-Bellman equations), finance (option pricing) or high-dimensional parameter spaces.

Analytically, it may be interesting to investigate the case of “escaping the native space” [28], i.e. the case where the target function is coarser than the used kernel and it may be interesting to see how the convergence rates degrade depending on the difference in the smoothness between the kernel and the solution.

Methodologically, it seems evident that problem specific kernels have the potential to provide very compact models. Thus it seems immediate to extend the present greedy kernel collocation approach with multilayer or deep-kernel learning in the spirit of [44, 45]. For problems with structural invariances, it may be promising to use structure-preserving kernels in the position component, e.g., divergence-free kernels [14, 43] for incompressibility conditions.

## Acknowledgements

The authors acknowledge the funding of the project by the Deutsche Forschungsgemeinschaft (DFG, German Research Foundation) under number 540080351 and Germany’s Excellence Strategy - EXC 2075 - 390740016.

## Appendix A Proofs of Propositions

*Proof of Proposition 3.* Without loss of generality, we assume

$$P_{\Lambda_0}(\lambda) \leq 1 \text{ for all } \lambda \in \Lambda. \quad (12)$$

If this condition is not met, the boundedness of  $\Lambda$  implies the existence of a factor such that the scaling of the functionals ensures (12). The proof then continues with the scaled functionals and the scaling factor enters the final constant  $C$  in the decay rate. With (12) the assumptions of Thm. 17 in [48] are valid and from its proof we cite the bound (using  $\bar{n}$  and  $\bar{C}$  to discriminate from the variables in the proposition)

$$\min_{i=\bar{n}+1, \dots, 2\bar{n}} \sup_{\lambda \in \Lambda} |\lambda(u - s_i)| \leq \bar{C} \bar{n}^{-\beta/2} \bar{n}^{-\alpha} \|e_{\bar{n}+1}\|_{\mathcal{H}_k(\bar{\Omega})} \log(\bar{n})^\alpha, \quad (13)$$

which is valid for  $\bar{n} \geq 3$ . As  $e_{\bar{n}+1} = u - s_{\bar{n}+1}$  and  $s_{\bar{n}+1}$  is obtained as an orthogonal projection we conclude by Pythagoras that  $\|e_{\bar{n}+1}\| \leq \|u\|$ . On the left hand side the minimum can be lower bounded by taking the minimum over all  $i = 1, \dots, 2\bar{n}$  instead of considering the smaller range  $i = \bar{n} + 1, \dots, 2\bar{n}$ . We abbreviate  $\gamma := -\beta/2 + 1/2 - (\tau - 2)/d < 0$ . For odd  $n = 2\bar{n} + 1$  we obtain

$$\bar{n}^\gamma = \left(\frac{n-1}{2}\right)^\gamma = \left(\frac{1}{2}\right)^\gamma \left(1 - \frac{1}{n}\right)^\gamma n^\gamma. \quad (14)$$



Assuming  $\bar{n} \geq 3$  we have  $n \geq 7$  and can upper bound the middle factor by  $\left(\frac{6}{7}\right)^\gamma$  and define the new constant as

$$C := \bar{C} \left(\frac{1}{2}\right)^\gamma \left(\frac{6}{7}\right)^\gamma = \bar{C} \left(\frac{3}{7}\right)^\gamma.$$

Further the logarithm factor can be upper bounded by  $\log(\bar{n}) < \log(2\bar{n} + 1) = \log(n)$ . Thus we overall verify the statement for odd  $n$  as  $\min_{i=1, \dots, n}(\cdot) = \min_{i=1, \dots, 2\bar{n}+1}(\cdot) \leq \min_{i=1, \dots, 2\bar{n}}(\cdot)$  and using (13) with (14). For even  $n = 2\bar{n}$  we similarly obtain

$$\bar{n}^\gamma = \left(\frac{n}{2}\right)^\gamma = \left(\frac{n}{2}\right)^\gamma = \left(\frac{1}{2}\right)^\gamma n^\gamma \quad (15)$$

which then is similarly resembled by the new constant  $C$  and overall gives the statement for all  $n \geq 6$ .  $\square$

*Proof of Proposition 5.* We argue very analogously to the previous proof, hence shorten the presentation: We start with a bound obtained in [41] using  $\bar{n}$ , etc. to discriminate from the present notation:

$$\min_{i=\bar{n}+1, \dots, 2\bar{n}} \sup_{\lambda \in \Lambda} |\lambda(u - s_i)| \leq \bar{C} \bar{n}^{-1/2} \|u - s_{\bar{n}+1}\|_{\mathcal{H}_k(\bar{\Omega})} e^{-\bar{c}_1 \bar{n}^{\frac{1}{2d}}}.$$

We can lower bound the RHS by extending the index range from  $i = 1, \dots, 2\bar{n}$ . The error norm on the RHS can again be upper bounded by  $\|u\|_{\mathcal{H}_k(\bar{\Omega})}$ . For the even case  $n := 2\bar{n}$  the exponent in the last factor on the RHS can be rewritten as

$$-\bar{c}_1 \bar{n}^{\frac{1}{2d}} = -\bar{c}_1 \left(\frac{n}{2}\right)^{\frac{1}{2d}} = -\bar{c}_1 \left(\frac{1}{2}\right)^{\frac{1}{2d}} n^{\frac{1}{2d}} = -c_1 n^{\frac{1}{2d}}$$

by setting  $c_1 := \bar{c}_1 \left(\frac{1}{2}\right)^{\frac{1}{2d}}$ . As in (15) but using a different  $\gamma$  the factor  $\bar{n}^\gamma$  can be expressed by a corresponding constant factor and  $n^\gamma$ . In the case of odd  $n = 2\bar{n} + 1$  similar reformulations and upper bounding according to (14) can be applied requiring that  $n$  is sufficiently large, e.g.  $n \geq 6$ . The statement then follows by suitable definition of the constant  $C$ .  $\square$

## References

- [1] K. Albrecht, J. Entzian, and A. Iske. Product kernels are efficient and flexible tools for high-dimensional scattered data interpolation. *Advances in Computational Mathematics*, 51(2):14, Mar 2025.
- [2] K. Albrecht and A. Iske. On the convergence of generalized kernel-based interpolation by greedy data selection algorithms. *BIT Numerical Mathematics*, 65(1):5, Dec 2024.
- [3] N. Aronszajn. Theory of reproducing kernels. *Transactions of the American Mathematical Society*, 68:337–404, 1950.
- [4] P. Batlle, Y. Chen, B. Hosseini, H. Owhadi, and A. M. Stuart. Error analysis of kernel/GP methods for nonlinear and parametric PDEs. *Journal of Computational Physics*, 520:113488, 2025.

- [5] P. Benner, S. Gugercin, and K. Willcox. A survey of projection-based model reduction methods for parametric dynamical systems. *SIAM Review*, 57(4):483–531, jan 2015.
- [6] Y. Chen and S. Gottlieb. Reduced collocation methods: Reduced basis methods in the collocation framework. *Journal of Scientific Computing*, 55:718–737, 2013.
- [7] Y. Chen, B. Hosseini, H. Owhadi, and A. M. Stuart. Solving and learning nonlinear PDEs with Gaussian processes. *Journal of Computational Physics*, 447:110668, 2021.
- [8] P. Constantine. *Active Subspaces: Emerging Ideas for Dimension Reduction in Parameter Studies*. Spotlights. SIAM, Philadelphia, USA, 2015.
- [9] O. Davydov and D. T. Oanh. Adaptive meshless centres and RBF stencils for Poisson equation. *Journal of Computational Physics*, 230(2):287–304, 2011.
- [10] S. De Marchi, R. Schaback, and H. Wendland. Near-optimal data-independent point locations for radial basis function interpolation. *Advances in Computational Mathematics*, 23(3):317–330, 2005.
- [11] S. Dutta, M. W. Farthing, E. Perracchione, G. Savant, and M. Putti. A greedy non-intrusive reduced order model for shallow water equations. *Journal of Computational Physics*, 439:110378, 2021.
- [12] G. E. Fasshauer. Solving partial differential equations by collocation with radial basis functions. In *Surface Fitting and Multiresolution Methods*, pages 131–138. Vanderbilt University Press, Nashville, USA, 1997.
- [13] G. E. Fasshauer, F. J. Hickernell, and H. Wozniakowski. On dimension-independent rates of convergence for function approximation with Gaussian kernels. *SIAM Journal on Numerical Analysis*, 50(1):247–271, 2012.
- [14] E. Fuselier, F. Narcowich, J. Ward, and G. Wright. Error and stability estimates for surface-divergence free RBF interpolants on the sphere. *Mathematics of Computation*, 78(268):2157–2186, 2009.
- [15] C. Greif and K. Urban. Decay of the Kolmogorov N-width for wave problems. *Applied Mathematics Letters*, 96:216–222, 2019.
- [16] B. Haasdonk. Reduced Basis Methods for Parametrized PDEs – A Tutorial Introduction for Stationary and Instationary Problems. In P. Benner, A. Cohen, M. Ohlberger, and K. Willcox, editors, *Model Reduction and Approximation: Theory and Algorithms*, pages 65–136. SIAM, Philadelphia, 2017.
- [17] B. Haasdonk and G. Santin. Approximation and data-analysis with kernels, 2025.
- [18] J. Hesthaven, G. Rozza, and B. Stamm. *Certified Reduced Basis Methods for Parametrized Partial Differential Equations*. SpringerBriefs in Mathematics. Springer, Switzerland, 2016.

- [19] E. J. Kansa. Multiquadrics — A scattered data approximation scheme with applications to computational fluid-dynamics. II. Solutions to parabolic, hyperbolic and elliptic partial differential equations. *Computers & Mathematics with Applications*, 19(8-9):147–161, 1990.
- [20] C.-F. Lee, L. Ling, and R. Schaback. On convergent numerical algorithms for unsymmetric collocation. *Adv. Comput. Math.*, 30(4):339–354, 2009.
- [21] E. Lehto, V. Shankar, and G. B. Wright. A radial basis function (RBF) compact finite difference (FD) scheme for reaction-diffusion equations on surfaces. *SIAM Journal on Scientific Computing*, 39(5):A2129–A2151, 2017.
- [22] L. Ling, R. Opfer, and R. Schaback. Results on meshless collocation techniques. *Engineering Analysis with Boundary Elements*, 30(4):247 – 253, 2006.
- [23] L. Ling and R. Schaback. On adaptive unsymmetric meshless collocation. In *Proceedings of the 2004 International Conference on Computational & Experimental Engineering and Sciences (Forsyth, USA)*, 2004.
- [24] L. Ling and R. Schaback. Stable and convergent unsymmetric meshless collocation methods. *SIAM J. Numer. Anal.*, 46(3):1097–1115, 2008.
- [25] L. Ling and R. Schaback. An improved subspace selection algorithm for meshless collocation methods. *Internat. J. Numer. Methods Engrg.*, 80(13):1623–1639, 2009.
- [26] Y. Maday, O. Mula, and G. Turinici. Convergence analysis of the generalized empirical interpolation method. *SIAM Journal on Numerical Analysis*, 54(3):1713–1731, 2016.
- [27] S. Müller. *Komplexität und Stabilität von kernbasierten Rekonstruktionsmethoden (Complexity and Stability of Kernel-based Reconstructions)*. PhD thesis, Fakultät für Mathematik und Informatik, Georg-August-Universität Göttingen, 2009.
- [28] F. J. Narcowich, J. D. Ward, and H. Wendland. Sobolev error estimates and a Bernstein inequality for scattered data interpolation via radial basis functions. *Constructive Approximation*, 24(2):175–186, Sep 2006.
- [29] A. Nouy. A priori model reduction through Proper Generalized Decomposition for solving time dependent partial differential equations. *Computer Methods in Applied Mechanics and Engineering*, 199(23–24):1603–1626, 2010.
- [30] D. T. Oanh, O. Davydov, and H. X. Phu. Adaptive RBF-FD method for elliptic problems with point singularities in 2d. *Applied Mathematics and Computation*, 313:474–497, 2017.
- [31] M. Ohlberger and S. Rave. Reduced basis methods: Success, limitations and future challenges. *Proceedings of the Conference Algoritmy*, pages 1–12, 2016.

- [32] M. Raissi, P. Perdikaris, and G. E. Karniadakis. Physics informed neural networks: A deep learning framework for solving forward and inverse problems involving nonlinear partial differential equations. *Journal of Computational Physics*, 378:686–707, 2019.
- [33] M. Renardy and R. C. Rogers. *An introduction to partial differential equations*, volume 13. Springer Science & Business Media, New York, USA, 2006.
- [34] G. Santin, T. Wenzel, and B. Haasdonk. On the optimality of target-data-dependent kernel greedy interpolation in Sobolev reproducing kernel Hilbert spaces. *SIAM Journal on Numerical Analysis*, 62(5):2249–2275, 2024.
- [35] R. Schaback. Convergence of unsymmetric kernel-based meshless collocation methods. *SIAM Journal on Numerical Analysis*, 45(1):333–351, 2007.
- [36] R. Schaback. A greedy method for solving classes of PDE problems. *arXiv preprint arXiv:1903.11536*, 2019.
- [37] R. Schaback and H. Wendland. Adaptive greedy techniques for approximate solution of large RBF systems. *Numerical Algorithms*, 24(3):239–254, 2000.
- [38] V. Shankar, R. M. Kirby, and A. L. Fogelson. Robust node generation for mesh-free discretizations on irregular domains and surfaces. *SIAM Journal on Scientific Computing*, 40(4):A2584–A2608, 2018.
- [39] P. Suchde, T. Jacquemin, and O. Davydov. Point cloud generation for meshfree methods: An overview. *Archives of Computational Methods in Engineering*, 30(2):889–915, Mar 2023.
- [40] O. Vlasiuk, T. Michaels, N. Flyer, and B. Fornberg. Fast high-dimensional node generation with variable density. *Computers & Mathematics with Applications*, 76(7):1739–1757, 2018.
- [41] P. Vogel. Target dependent greedy sampling for Gaussian kernel PDE collocation, 2024. SimTech B.Sc. Thesis, University of Stuttgart.
- [42] H. Wendland. *Scattered Data Approximation*, volume 17 of *Cambridge Monographs on Applied and Computational Mathematics*. Cambridge University Press, Cambridge, 2005.
- [43] H. Wendland. Divergence-free kernel methods for approximating the Stokes problem. *SIAM Journal on Numerical Analysis*, 47(4):3158–3179, 2009.
- [44] T. Wenzel, B. Haasdonk, H. Kleikamp, M. Ohlberger, and F. Schindler. Application of deep kernel models for certified and adaptive RB-ML-ROM surrogate modeling. In *Large-Scale Scientific Computations*, number 13952 in LNCS, pages 117–125. Springer, Cham, Switzerland, 2024.
- [45] T. Wenzel, F. Marchetti, and E. Perracchione. Data-driven kernel designs for optimized greedy schemes: A machine learning perspective. *SIAM Journal on Scientific Computing*, 46(1):C101–C126, 2024.

- [46] T. Wenzel, G. Santin, and B. Haasdonk. A novel class of stabilized greedy kernel approximation algorithms: Convergence, stability and uniform point distribution. *Journal of Approximation Theory*, 262:105508, 2021.
- [47] T. Wenzel, G. Santin, and B. Haasdonk. Analysis of target data-dependent greedy kernel algorithms: Convergence rates for  $f$ -,  $f \cdot P$ - and  $f/P$ -greedy. *Constructive Approximation*, 57(1):45–74, 2023.
- [48] T. Wenzel, D. Winkle, G. Santin, and B. Haasdonk. Adaptive meshfree approximation for linear elliptic partial differential equations with PDE-greedy kernel methods. *BIT Numerical Mathematics*, 65(1), 2025.
- [49] D. Wirtz and B. Haasdonk. A vectorial kernel orthogonal greedy algorithm. *Dolomites Research Notes on Approximation*, 6:83–100, 2013.